ACS APPLIED MATERIALS & INTERFACES

www.acsami.org

Research Article

Large-Scale Selective Micropatterning with Robotics nDEP Tweezers and Hydrogel Encapsulation

Kaicheng Huang, Jiewen Lai, Hongliang Ren, Chunhui Wu, Xing Cheng, and Henry Kar Hang Chu*

Cite This: *ACS Appl. Mater. Interfaces* 2024, 16, 49973−49984

Read Online

ACCESS | Metrics & More | Article Recommendations

ABSTRACT: Creating diverse microparticle patterns on a large scale enhances the performance and efficiency of biochemical analytics. Current techniques exhibit limitations in achieving diverse microparticle patterns on a large scale, primarily focusing on patterning particles of the same type with limited flexibility and accessibility. Moreover, accessibility to patterned particles without a fixed formation poses additional challenges. Herein, in this work, we introduce a novel robotic micropatterning system designed to address these challenges. The system facilitates the selection, batch transferring, patterning, and encapsulation of microparticles using negative dielectrophoresis (nDEP)-tweezers, enabling large-scale microparticle patterning on a hydrogel. A multielectrode chip was mounted on a micromanipulator to serve as the nDEP tweezers, and the microparticles scattering on the substrate could be trapped and displaced to different positions on a substrate with an array of holes for large-scale pattern generation. Photosensitive hydrogel was employed for microparticle pattern encapsulation. The effects of configuring different experimental parameters on the patterning efficiency were evaluated and analyzed. Experiments were conducted to explore the stability and performance of the micropatterns. Various patterns with hydrogel encapsulation were created using different color polystyrene microbeads (orange, blue, and green) with varying sizes (50, 100, and 125 μm) under the adjusted environment. Results demonstrate the successful creation of large-scale microbead patterns in a specified form and their encapsulation into an extractable hydrogel using the proposed nDEP tweezer system. The proposed system can be potentially applied to diverse bioparticles for analysis.

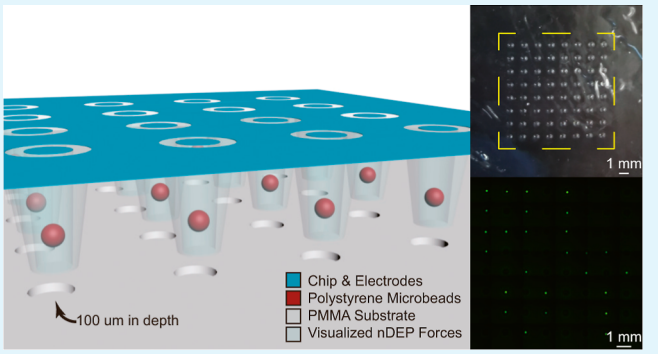

KEYWORDS: *automatic control, dielectrophoresis, micro- and nanoscales, micropatterning, micromanipulation*

INTRODUCTION

Microparticle patterning technology is of great importance in biology and pharmaceutical analytics. It arranges various microbioparticles in arrays through micromanipulation methods, enabling advancements in research and applications such as rapid single-cell analysis,[1−4] immunoassays,[5] biological particle detection,[6,7] and drug testing.[8,9] Large-scale microparticle patterning can significantly enhance the development process by enabling high-throughput screening, precise control over experimental conditions, and the creation of complex, multicomponent assays. It can facilitate high-throughput analysis by arranging microparticles in an array through micromanipulation methods allowing for simultaneous testing in an array format. This can speed up the process of studying interactions with particle targets. For example, large-scale microparticle patterning can be used in combinatorial chemistry to synthesize and screen large libraries of related compounds. This can aid in the discovery of new drug candidates with improved potency and selectivity.[10] To accelerate the research and development cycle in biochemical analysis studies, researchers have begun using microcolloidal particles for many proof-of-concept tasks, as these particles can be tailored to different sizes to mimic various cell types.[11] Additionally, engineered colloidal particles can serve as agents in biological sensing, including immunosensing,[12−16] protein−protein interactions,[17−19] cell targeting,[11,20] and cell pairing.[21] Therefore, microcolloidal particle patterning has gained significant attention in recent years.

Microparticle manipulation is an important technique used to facilitate microcolloidal particle patterns. In the field, lab-on-a-chip (LOC) devices have been widely employed because they are cost-effective and easy to fabricate compared with traditional laboratory methods.[22] In general, a millimeter-scale

Received: June 27, 2024
Revised: August 28, 2024
Accepted: August 30, 2024
Published: September 4, 2024

LOC device with microchannels can be fabricated using lithography.[23] The operating principle of an LOC device is to apply noncontact force, such as magnetic,[24] electrical,[25−28] hydrodynamic,[29] acoustic,[30] or gravitational force, on microparticles within the microchannel. For magnetic force manipulation, the target particles must possess magnetic properties. In cases where the particles are not inherently magnetic, a pretreatment process is required to render them magnetic. However, this process may introduce chemicals that could be detrimental to biological entities such as cells. With respect to electrical force manipulation, this technique is applicable only to particles that are electrically charged. Hydrodynamic, acoustic, and gravitational forces necessitate sophisticated control systems to achieve effective particle manipulation. Among all, dielectrophoresis (DEP) force is a commonly employed technique for particle patterning,[31−36] because DEP-based LOC devices can be conveniently fabricated. Importantly, DEP force manipulation is universally applicable to a broad spectrum of biological cells, which are inherently polarizable.[37] This approach eliminates the need for pretreatment, thus, reducing the risk of potential harm to the cells. The fabrication process of a DEP-based LOC device involves bonding a polydimethylsiloxane cover to a glass substrate, forming a microchannel. The glass substrate with deposited electrodes serves as the microchip.[38] Within the microchannel, a nonuniform electric field generated by the electrode causes the particles to experience a DEP force.[39] With an electrode array, microparticle patterning can be formed within the DEP-based LOC device.[13,16,17,40]

It is worth noting that while LOC devices can be easily fabricated, some devices are specifically designed to cater to specific applications, requiring unique channel structures to facilitate the desired patterning outcomes. For example, Wu et al.[21] have designed a DEP-based LOC device for cell pairing. Cells in the channel were patterned based on the size of the cell. Although this device can achieve cell pairing, it can be applied only to specific cell types. Universal patterning systems were also studied by holding microparticles with a DEP force. Menad et al.[41] used a bottom-up structure LOC device to aggregate cell cluster patterns with negative-DEP force. Yafouz et al.[42] used dot micro array dot electrodes to form a microparticle array. These studies demonstrate the versatility of LOC devices in creating different patterns for various applications, where the size of these micropatterns is indeed restricted by the size of the electrode arrays. Therefore, a flexible patterning system should be fabricated to overcome this constraint and broaden the application scope of LOC devices.

In addition, particles entrapped or immobilized on the substrate of the microchannel cannot be detached in pattern forms for further process. The immobilization and detachment of particles from the microchannel substrate present challenges that must be addressed. Particles can only be obtained by washing them from the microchannel through microfluidics and collecting them from the microchannel. To get an intact microparticle pattern, trapping and encapsulating DEP-patterned microparticles in a photosensitive hydrogel have been reported to immobilize and peel off the particle pattern from the LOC device after processing.[43−51] Poly(ethylene glycol) diacrylate (PEG-DA) is commonly used for microparticle pattern encapsulation.[43−46,48−50,52] Mixing with the photoinitiator (2-hydroxy-2-methylpropiophenone), the hydrogel solution was cured after exposure to ultraviolet light. However, the curing hydrogel can be removed only by destroying the whole LOC device as the device is fully sealed, which increases the cost and complexity of the process, as the microchannel is fabricated in an irreversible way. To overcome these challenges, Zhang et al.[53] have designed a reversible LOC device. In this device, a 50 μm-thick Teflon film is used as a spacer, and a thin glass sheet covers the microchip. This allows the PEG-DA hydrogel with patterned microparticles to be easily peeled off as the LOC device is easily detached. However, a hydrophobic layer may be necessary to protect the cured hydrogel from damage during peeling in a closed environment. Another approach to simplifying the whole process is to encapsulate patterned particles in an open environment, which can potentially reduce the need for specialized equipment and allow for easier manipulation of the particles. This open-environment approach can be particularly useful for applications that require the patterned particles to be easily accessible for further processing or analysis.

This article introduces a micromanipulation system designed to pattern large-scale microparticles utilizing a limited number of electrode microchips and subsequently encapsulate the patterned microparticles within a hydrogel in an open setting. The proposed system enables facile detachment of the hydrogel containing the large-scale microparticle pattern. Comprising five key components, the system includes an inversely equipped microchip with electrodes connected to a relay-controlled function generator, a three-dimensional (3D) micromanipulator equipped with a microchip holder for precise adjustment of microchip positioning, a poly(methyl methacrylate) (PMMA) substrate featuring an 8 × 8 array of holes, a motorized stage for substrate displacement, and an inverted microscope.

The microchip serves as multiple negative DEP (nDEP) tweezers, generating numerous electric fields for simultaneous trapping and manipulation of microparticles.[54] The gap or microchannel between the microchip and the substrate can be precisely controlled, and the microchip is easily detached, offering superior advantages over conventional LOC devices. Microscope images aid in precise alignment and manipulation among the beads, microchips, and substrate. The system was employed to create small polystyrene (PS) bead patterns in previous research.[55] By selectively energizing the electrodes, the beads were driven underneath each energized electrode, forming diverse patterns via nDEP. In this study, the system was modified to generate a large-scale bead pattern encapsulated within the hydrogel. PEG-DA solution containing beads was dispensed onto the substrate. The electric fields were generated from the microchip to trap and transfer the selected bead onto the substrate and form a microbead pattern. Utilization of a PMMA substrate with an 8 × 8 array of holes minimizes flow-induced perturbations on the transferred bead pattern and aids in large-scale pattern formation. Following the formation of the large-scale bead pattern, UV-light exposure facilitates curing of the solution. Experimental optimizations were conducted to enhance the patterning efficiency and stability of the bead pattern prior to curing, thereby increasing the overall success rates. PS bead patterns with single, double, and triple colors were generated, showing the availability of the system for patterning various types of microparticles. Additionally, hexagonal and octagonal PS bead patterns were fabricated, showcasing the system's ability to pattern different microparticles into specified forms. Given the ubiquitous applicability of DEP in manipulating microparticles, the

https://doi.org/10.1021/acsami.4c10675
ACS Appl. Mater. Interfaces 2024, 16, 49973−49984

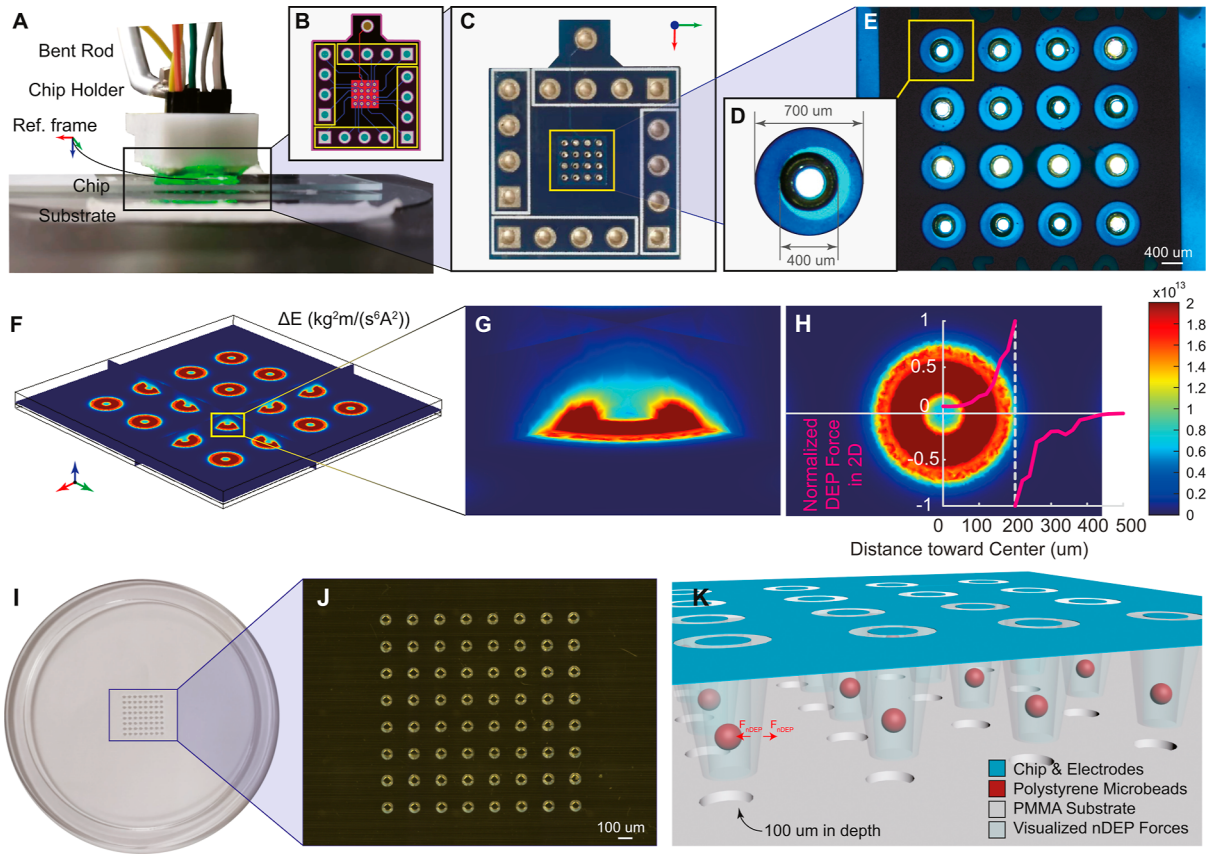

Figure 1. System description. (A) The chip (nDEP tweezers) is held by a bent rod connected to a micromanipulator, while the substrate is placed beneath the chip. An inverted microscope obtains the microscopic view. (B) Electronic design and wiring schematics of the nDEP tweezers. (C) PCB prototype of the chip. (D) Dimension of a single nDEP-tweezer node. (E) Microscopic view of the functional area of the chip. (F) Electric field simulation of the chip. (G) Zoom-in local view of the electric field simulation of a single electrode. (H) Top view of the electric field simulation of a single electrode, with its normalized DEP force against distance toward the electrode center. (I) Snapshot of the 3D-printed PMMA substrate with 8-by-8 hole arrays, and (J) its microscopic view. (K) Schematic of the working area that includes the chip, PS microbeads, substrate, and the visualized field of nDEP forces. The robotized nDEP field can selectively trap the microbead for large-scale translational motion.

envisaged utilization of the system pertains to the conduct of analysis on a diverse array of biological particles such as cells, enabling large-scale cell monitoring, cell migration, and chemotaxis studying and external signal respond studying.

EXPERIMENTAL SECTION

Principle of DEP. The central component of the system comprises a multilayer chip employing the DEP technique to generate nonuniform electric fields via electrodes positioned at distinct layers, facilitating manipulation and trapping of microparticles.[56] Findings as documented by Pohl[57] demonstrate that all microparticles could be polarized in a spatially nonuniform electric field. The induced dipole moment in the particle results in a net DEP force propelling the particle within the nonuniform electric field environment. The evaluation of the force acting on the particles $\boldsymbol{F}_{\mathrm{DEP}}$ can be described as follows

$$\boldsymbol{F}_{\mathrm{DEP}} = 2\pi r^3 \varepsilon_{\mathrm{m}} \cdot Re[K(\omega)] \cdot \nabla E^2 \quad (1)$$

where r is the radius of the particle, ε_{m} is the permittivity of the suspending medium, ∇ denotes the Del vector operator, E is the root-mean-square of the electric field, and $Re[K(\omega)]$ is the real part of the Clausius−Mossotti factor that can be calculated as follows

$$K(\omega) = \frac{\varepsilon_{\mathrm{p}}^* - \varepsilon_{\mathrm{m}}^*}{\varepsilon_{\mathrm{p}}^* + 2\varepsilon_{\mathrm{m}}^*} \quad (2)$$

where $\varepsilon_{\mathrm{p}}^*$ and $\varepsilon_{\mathrm{m}}^*$ are the complex permittivity of the particle and suspension medium, respectively.

The direction of the force exerted on the particle is contingent on the gradient of the electric field and the relative polarizability between the particle and surrounding medium. The relative polarizability is based on the electrical properties of the medium and particle (conductivity and relative permittivity). The phenomenon of particles driven from the weak electric field toward the strong electric field is called positive DEP, whereas particles driven in the opposite direction are called nDEP. In the context of the chip being inversely positioned against the substrate, the utilization of nDEP force becomes essential to drive the beads toward the substrate underneath the electrodes, thereby facilitating their arrangement and patterning onto the substrate. Based on the experimental findings from our prior investigation,[56] the signal frequency utilized in this study was set above 8 MHz to induce nDEP force in the microbeads while mitigating the occurrence of electrolysis. As DEP forces can be applied in various microparticles, the proposed system can be employed for the pattern formation of diverse bioparticles by adjusting the frequency of the input signal.

Design of the Micropatterning System. The core component of the system is an nDEP tweezer that can generate ring-like electric fields within the microenvironment. Details on the design and fabrication of the nDEP tweezers are further described in the work by Huang et al.[55] In brief, the nDEP tweezers utilize a printed circuit board (PCB) plate as the surrounding electrode with 16 holes arranged in a four-by-four manner. As shown in Figure 1B−E, 16 circle electrodes are concentrically aligned with the holes on the plate, forming electrode pairs for PS bead manipulation via DEP electric

https://doi.org/10.1021/acsami.4c10675
ACS Appl. Mater. Interfaces 2024, 16, 49973−49984

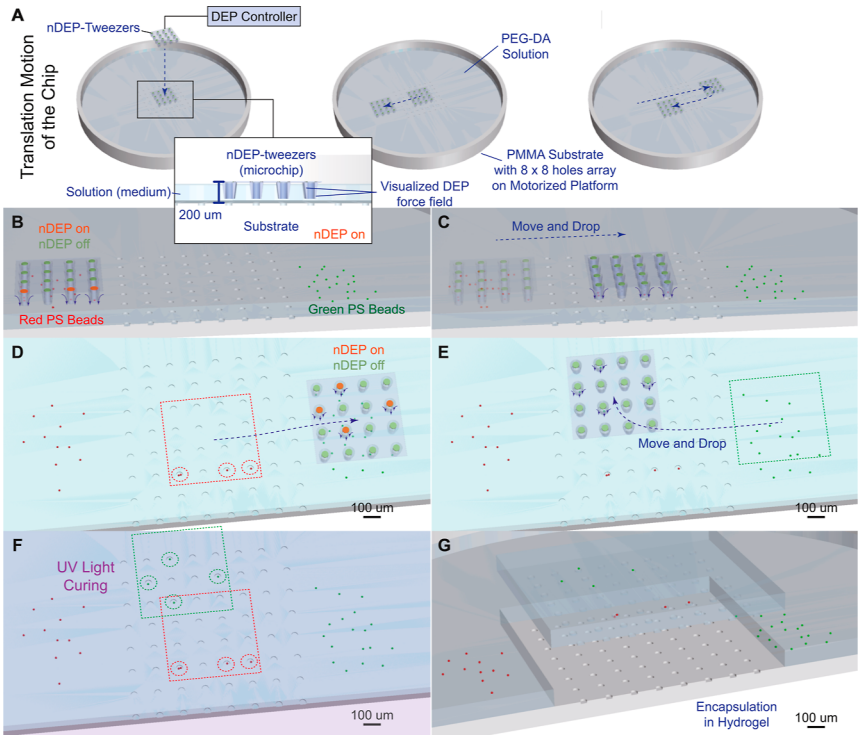

Figure 2. Schematics of microbead patterning and hydrogel encapsulation workflow using nDEP tweezers. (A) PEG-DA solution with scattering beads is dispensed on a 3D-printed PMMA substrate with hole arrays, and the chip can be positioned in space. A feasible working distance between the chip and the substrate is 200 μm. (B,C) First, the PEG-DA solution with red and green PS beads is injected into the PEG-DA solution on each side of the chip. Then, the tweezer moves toward the scattered red beads and selectively captures them with nDEP force. After that, the red beads are transferred and released to the hole array for stabilizing and forming the first batch of micropatterns. (D,E) The tweezer moves toward the scattered green beads and selectively picks the desired beads, then repeats the same patterning workflow. (F) The nDEP tweezer is lifted away from the PEG-DA solution; then, the UV light is used for PEG-DA curing—which as a result, encapsulates the well-patterned microbeads. (G) The center part of the solidified hydrogel with a bead-based pattern is subtracted and taken off.

fields. The distance between two adjacent electrodes is 1400 μm to prevent the bead from being trapped in the diamond-like zones formed by four adjacent electrodes. Preliminary validations on a commercial simulation platform (see Figure 1F–H) suggest that the nDEP tweezers we designed can effectively generate ring-like electric fields within the microenvironment. In particular, the relationship between the normalized DEP force acting on the particle and the distance between the particle and electrode is detailed in Figure 1H, depicting that the proposed tweezers can drive the surrounding microparticles toward the center of each electrode and hold the particles. A robotic-aided method was introduced to achieve precise micropatterning. The nDEP-tweezer chip was mounted on a 3-DOF micromanipulator through a 3D-printed chip holder to provide precise alignment between the chip and substrate surface (Figure 1A). A motorized vertical stage was used to adjust the objective lens. A vision-based algorithm was applied to the system to precisely position the microchip 200 μm above the substrate by monitoring the image sharpness. We utilize microcontroller-based relays to energize individual electrodes, induce the electric field to the selective trapping of microbeads, and realize logical programmability. A microscope (Leica DMi8) was used to visualize the manipulation site.

To maintain the patterned beads, a PMMA substrate with a 20 mm radius was fabricated through 3D printing, as shown in Figure 1I,J. The substrate features a central grid of holes arranged in an 8 × 8 pattern, each hole having a diameter of 500 μm and a height of 100 μm. To match the dimensions of the electrodes on the microchip, the distance between adjacent holes was set at 1400 μm. The PMMA substrate was placed on the motorized platform stage in the microscope system to position the substrate underneath the microchip. The correlated movement between the microbeads and microchip was induced by the motorized platform of the microscope to maintain the microchip within the region of interest. The platform position could be controlled by using a computer. The patterned microbeads were transferred to the holes in the PMMA substrate for encapsulation (Figure 1F).

Patterning Protocol. PEG-DA solution was poured and filled with the substrate. The microchip held by the micromanipulator was lowered to immerse in the solution with a 200 μm gap to the substrate, as shown in Figure 2A. The height of the microchip was precisely controlled through visual feedback. Different colored PS beads in the PEG-DA solution were used, and a droplet of each solution was dispensed at different substrate locations (Figure 2B). A detection program was used to obtain the relative positions and shape of electrodes within the field.[54] Through the movable stage at a speed of V, one type of microbead was first manipulated toward the bottom of each electrode for trapping. Depending on the pattern, the electrodes on the microchip could be selectively energized and turned on to hold the microbeads (Figure 2B). After bead trapping, the microchip with the bead pattern was transferred to the center of the substrate, and the electrodes were de-energized to release the beads onto the holes (Figure 2C). Repeating the procedure, another type of a PS bead pattern was also created (Figure 2D,E). After patterning several times, a large-scale microbead pattern was produced, and the microchip was moved upward for hydrogel curing by exposure of the substrate to UV light (Figure 2F). Finally, the central part of the hydrogel with a large-scale bead pattern was taken off (Figure 2G).

Patterning Procedure. To achieve two-color bead patterning, different colored beads were dispensed at the opposite side of the microchip, as shown in Figure 2. For single-bead pattern generation, an automatic separation method was developed and proposed in the previous study.[54] Through the motorized platform of the microscope system, by selectively turning on the individual electrode in the electrode array microchip, a micropattern can be created and held with electric fields via DEP force. The generated microbead pattern

https://doi.org/10.1021/acsami.4c10675
ACS Appl. Mater. Interfaces 2024, 16, 49973−49984

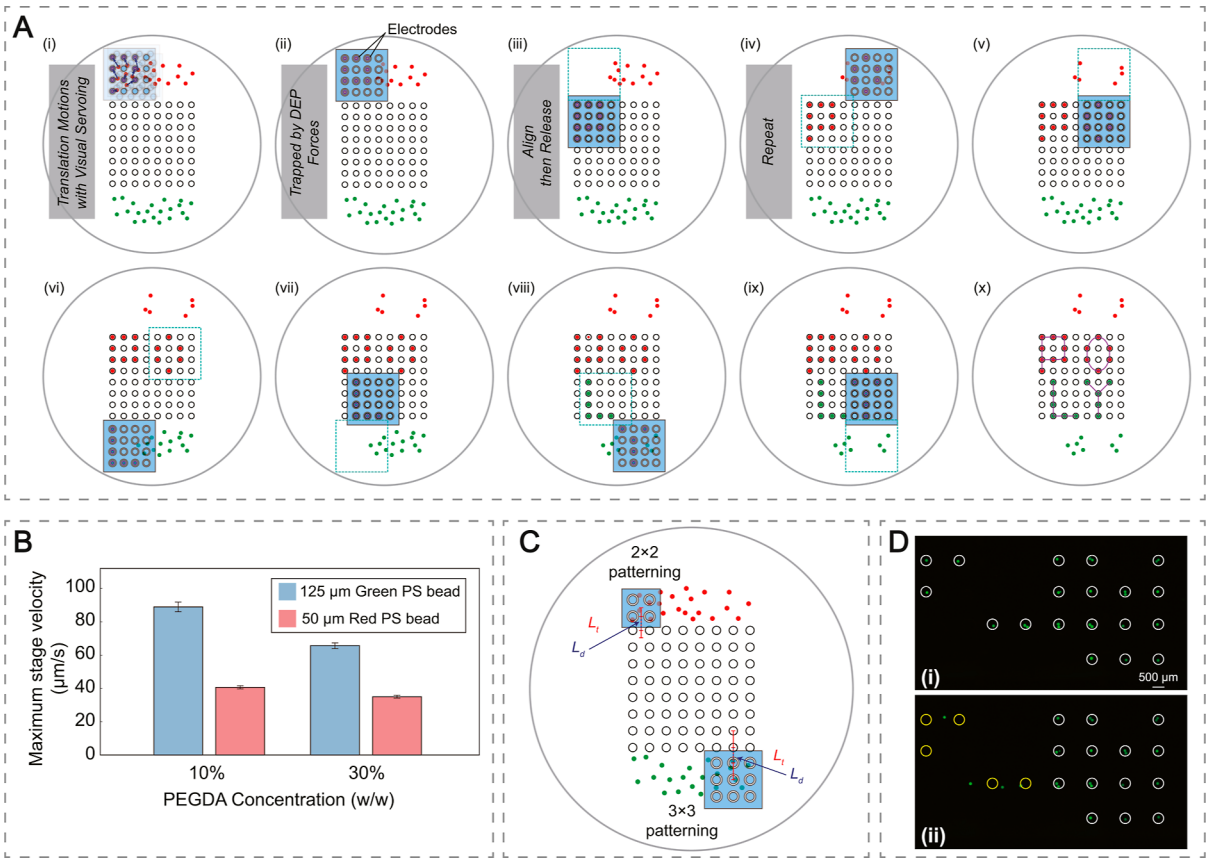

Figure 3. (A) Illustration of patterning red and green microbeads into designation characters via the programmable nDEP tweezers. (i) The red and green microbeads are arbitrarily scattered on either side of the substrate's patterned area. The nDEP tweezers capture the red beads via several translation motions guided by the visual servoing method and optimal algorithm for the most efficient path.[55] (ii) The nDEP tweezers capture sufficient microbeads and are ready for patterning. (iii) The tweezers align with the patterned substrate and release the microbeads. (iv–ix) Repeating the same workflow from A to C. (x) The desired pattern "POLY" is displayed on an 8-by-8 resolution pattern. (B) Maximum velocity for different size PS bead translation in different PEG-DA concentration solutions. (C) Illustration of different size patterning. (D) Illustration of quantifying the stability of the bead pattern. (i) Before lifting the microchip. (ii) After lifting the microchip.

was then transferred to the holes in the substrate for holding. Different pattern types can be created by controlling the relay and energizing different electrodes for holding the beads. The same procedure was applied to another color of PS beads and created a large-scale two-color pattern. The whole procedure is illustrated in Figure 3A.

Materials in the Experiment. PS beads were considered to create different patterns on the PMMA substrate. 700 Mn PEG-DA solution was mixed with 20% ethanol in water. During the experiments, the microbeads that gradually sunk to the bottom due to gravity resulted in an adhesion force that resisted movement. The introduction of PEG-DA would also increase the attachment phenomenon. To minimize the effect, polysorbate 20, also known as Tween 20, was used as a dispersant to reduce the adhesion force. The PS beads were added to the solution to reach a concentration of 0.02% w/v.

Micropattern Stability Evaluation. By randomly injecting PS bead solution in the center of the substrate and lowering the microchip, the microchip was lifted after 5 min and the performance of the bead pattern was observed by the microscope. To quantify the stability of the pattern, images of the pattern before and after lifting the microchip were captured and used to compute the bead attachment rate by counting the number of beads in the original place, as shown in Figure 3D. PS beads outside the circles are not in the hole array before moving the microchip and are neglected. The beads that are stable with the changing and with no decrease in amounts are circled in white, while there is a decline for the beads in the yellow circles. The lifting motion from the microchip would disrupt the environment, shifting beads away from their trapped positions on the substrate.

RESULTS AND DISCUSSION

Patterning Efficiency. In large-scale patterning, efficiency is important, as a long-time process would run out of the medium with evaporation. Therefore, the system was tested to decrease the patterning time and accelerate the whole process. A series of experiments were conducted to examine the performance of the proposed system for bead trapping. An appropriate stage velocity was selected, and the influence caused by the size of the pattern was also explored to obtain the maximum efficiency.

Selection in the Stage Velocity. The system introduced a relative motion between the microchip and substrate to create a relative motion between the microchip and microbeads. PS beads are subjected to drag force while moving in an aqueous environment. As the substrate moves at velocity V, it will create a motion in the fluid that follows a linear velocity profile along with the Y dimension, $\frac{\partial V}{\partial y}$. The induced shear stress (τ) acted equally with and oppositely from the fluid and substrate, with the following differential relation

$$\tau = \mu \frac{\partial V}{\partial y} \tag{3}$$

https://doi.org/10.1021/acsami.4c10675
ACS Appl. Mater. Interfaces 2024, 16, 49973−49984

Table 1. Simulation of Whole Patterning Time for $M \times M$ Resolution with $N \times N$ Patterning (10^2 s)

	$M = 2$	$M = 3$	$M = 4$	$M = 5$	$M = 6$	$M = 7$	$M = 8$
$N = 2$	0.5442	1.6326	2.1768	3.8094	4.8979	7.0747	8.7073
$N = 3$	1.2390	1.2390	2.4780	3.7170	4.9560	7.4340	9.9120
$N = 4$	2.0010	2.0010	2.0010	4.0020	6.0030	8.0040	8.0040
$N = 5$	3.3670	3.3670	3.3670	3.3670	6.7340	6.7340	10.1011
$N = 6$	5.1930	5.1930	5.1930	5.1930	5.1930	10.3861	10.3861
$N = 7$	7.2750	7.2750	7.2750	7.2750	7.2750	7.2750	15.5501
$N = 8$	9.5629	9.5629	9.5629	9.5629	9.5629	9.5629	9.5629

where μ is the viscosity of the medium.

With channel height h_c, the bead with a height of h is subjected to drag force induced by the fluid with a velocity of $\left(1 - \frac{h}{h_c}\right)V$. In this study, the PS beads were on the surface of the substrate due to the gravity force, where $h = 0$. To hold the PS beads firmly, the shear force acting on the beads must be equal to or less than the n-DEP force generated from the microchip ($\tau \leq F_{DEP}$). Therefore, the maximum velocity of the stage must satisfy the following equation

$$\mu V_{max}(2\pi r^2) = 2\pi r^3 \varepsilon_m \cdot Re[K(\omega)] \cdot \nabla E^2 \tag{4}$$

$$V_{max} = r\varepsilon_m \cdot Re[K(\omega)] \cdot \nabla E^2/\mu \tag{5}$$

where $2\pi r^2$ is the surface area of the half-spherical object.

According to eq 5, if the gradient of the electric field and electrical properties of the medium and particle are known, then the maximum velocity becomes directly related to the radius of the particle and the viscosity of the medium. To find a suitable stage moving velocity in a given voltage input, the relationship between the stage moving velocity, size of the PS beads, and concentration of PEG-DA was explored through experiments. First, a voltage was supplied to hold a bead on a substrate, and the substrate on the stage began to move at an increasing speed until the bead slid away.

The corresponding maximum velocity was recorded, and the results with different PEG-DA concentrations and different sizes of beads are shown in Figure 3B. The results confirm that as the viscosity of the medium decreases, a high-stage velocity can be used. Besides, the size of the particle would also influence the maximum velocity at which a larger bead can be transferred at a large velocity. Based on the results, a small concentration medium should be selected and reduce patterning time. For translation of the beads with a diameter of 50 and 125 μm, the stage velocities were set to 35 and 85 μm/s, respectively.

Size of the Pattern. Theoretically, the number of holes in the substrate can be increased to improve the resolution of the pattern. Meanwhile, the number of electrodes in the microchip can also be increased to improve the efficiency. However, it would take a longer time for the microchip to trap a single bead in each electrode. According to our previous research,[55] to achieve single-bead patterning with an $N \times N$ electrode array, the total time T_t can be expressed as follows

$$T_t = T_c + \frac{L_{min}}{V} \times \frac{d_e}{1/(N+1)} \tag{6}$$

where T_c is the computational time; L_{min} is the total moving distance traveled by the microchip to trap each electrode with a bead, which can be obtained through simulation using the ant colony optimization method discussed; V is the velocity of the platform, which is equal to 35; and d_e is the distance between the adjacent electrodes, which is equal to 1400 μm.

After trapping, the formed PS bead pattern is transferred to the center of the substrate for holding. With a traveling distance of L_t, the consuming time for one patterning cycle T_w can be calculated as

$$T_w = T_t + \frac{L_t}{V} \tag{7}$$

For the simplest case, the microchip can be directly transferred to where the holes are in a single dimension; as shown in Figure 3C, the traveling distance, L_t is decided by the size of the pattern. For an $N \times N$ pattern, the traveling distance L_t can be expressed as

$$L_t = (N-1)d_e + L_d \tag{8}$$

where L_d is the distance between the microchip to the desired location of the hole grid.

According to the previous study, in the patterning procedure, the time for single-bead holding and trapping dominates the patterning time. Therefore, the total time T_w for one cycle is

$$T_w = \frac{L_{min}(N+1) + (N-1)}{V} d_e + \frac{L_d}{V} \tag{9}$$

To fabricate a pattern with $M \times M$ resolution, assuming that L_d equals 0, the whole fabrication time is

$$T = \frac{L_{min}(N+1) + (N-1)}{V} d_e \times \left\lceil \frac{M^2}{N^2} \right\rceil \tag{10}$$

where L_{min} is based on a simulated environment with 2^8 beads, $\lceil\ \rceil$ is the ceiling function, and the whole fabrication time T is summarized in Table 1. When $M = aN$, where a is an integer ($M = 6$, $N = 2$; $M = 8$, $N = 4$), the fabrication time reaches its local minimum. Based on these results, to test if the total moving distance L_{min} or cycling time $\left\lceil \frac{M^2}{N^2} \right\rceil$ is dominant in the whole fabrication time, another simulation with a potentially increased number of electrode arrays and resolution ($M = 2^n$, $N = 2^n$) was also performed and is summarized in Table 2. Apparently, filling the chip with beads costs much more time

Table 2. Simulation of Whole Patterning Time for $M \times M$ Resolution with $N \times N$ Patterning, Where $M = 2^n$ s and $N = 2^n$ s (10^2 s)

	$M = 2$	$M = 4$	$M = 8$	$M = 16$
$N = 2$	0.556	2.2265	8.9058	35.6233
$N = 4$	2.2101	2.2101	8.8405	35.3621
$N = 8$	11.2686	11.2686	11.2686	45.0745
$N = 16$	127.6600	127.6600	127.6600	127.6600

https://doi.org/10.1021/acsami.4c10675
ACS Appl. Mater. Interfaces 2024, 16, 49973−49984

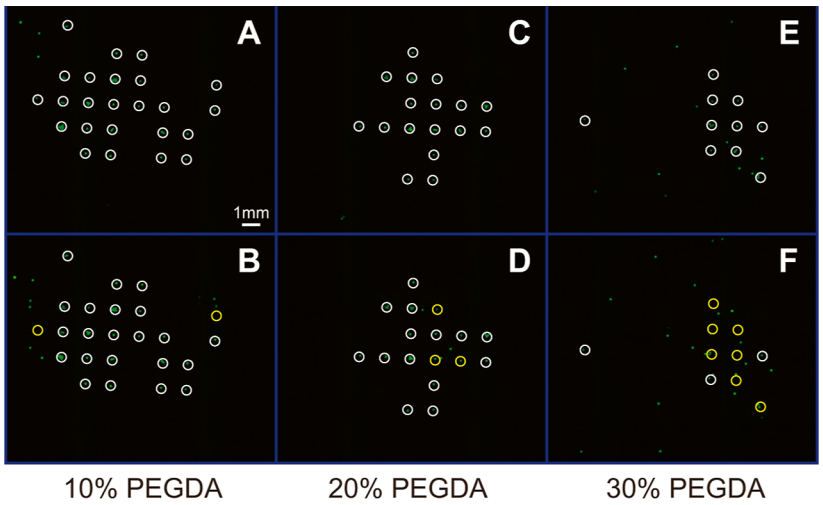

Figure 4. Microscopic images before and after the microchip is lifted up with a PEG-DA concentration of (A,B) 10, (C,D) 20, and (E,F) 30%.

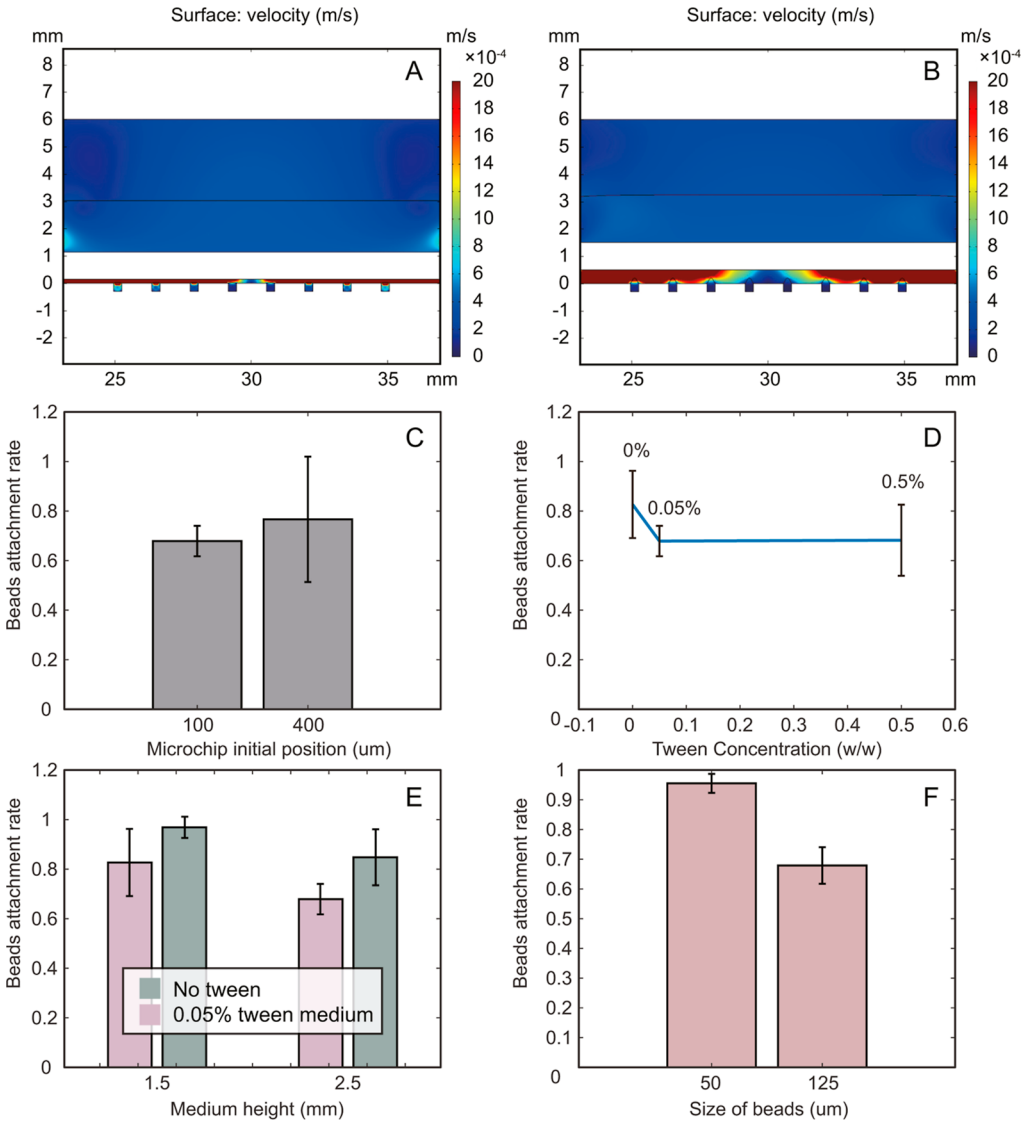

Figure 5. Simulations of the microchip being lifted up away from the medium with a medium height of (A) 1.5 and (B) 3 mm. Experimental results about pattern stability with different environments. (C) Different microchip initial position. (D) Different tween concentration. (F) Different medium height. (F) Different sizes of beads.

https://doi.org/10.1021/acsami.4c10675
ACS Appl. Mater. Interfaces 2024, 16, 49973−49984

than moving the patterned beads to the hole. It is preferable to use a smaller microchip to form a larger pattern with more cycles. Therefore, in this paper, to improve the patterning efficiency, for each cycle of patterning, the 2 × 2 electrode array would be used for PS bead trapping and translation.

Stability of a Micropattern. As described in the previous section, different from the conventional microfluidic device, the proposed system detaches the microchip from the substrate, offering an open environment (Tables 1 and 2). Therefore, the formed hydrogel can easily be removed from the substrate instead of the microfluid device. To cure the hydrogel solution, the microchip needs to be lifted and moved away from the solution. The movement of the microchip leads to chaos in the medium, which is also a reason for the use of holes to stabilize the beads. Simulations were performed to show the procedure. Different environments that would influence the stability of the pattern during the procedure were evaluated through experiments, ensuring that the beads were in the patterning form before hydrogel curing. The pattern quality is highly correlated to the medium, microchip, and beads. The bead attachment tests were conducted to examine the effects of individual parameters and optimize them.

Effect of the Medium Density. The density of the solution is one of the factors influencing the quality of the PS bead pattern. Beads gradually sink to the bottom of the holes because of the gravitational force. If the beads are suspended in a medium denser than the beads, then a high buoyancy force would levitate the beads, so that they cannot be transferred by the substrate. Also, a high-density medium would decrease the contact between beads and the substrate, which would lower the attachment force and lead to the instability of the bead pattern. The adhesion force was proportional to the normal force in the vertical direction F_t. Given that the bead in the medium would experience gravity F_g and buoyancy F_f in the vertical direction, the normal force F_t can be expressed as follows

$$F_t = F_g - F_f = \rho_p g V_p - \rho_m g V_p = (\rho_p - \rho_m) g V_p \quad (11)$$

where ρ_p and ρ_m are the density of the medium and bead, respectively; and V_p is the volume of the bead. In the system, a large medium density ρ_m would lead to a small normal force in the vertical direction F_t and result in a small adhesion force. Lifting the microchip would cause turbulent flow and disrupt the already-formed pattern. As the PS beads have a density of 1.05 g/cm^3, PEG-DA has a density of approximately 1.12 g/cm^3, and the concentration of the PEGDA solution was set lower than 41.6% to satisfy the requirement of $\rho_p \geq \rho_m$, preventing the PS beads from floating in the solution.

In this work, different PEG-DA concentrations would lead to different medium densities and their influence on the pattern. PEG-DA solutions were produced to prepare solutions with different concentrations from 10 to 30% to suspend the beads for evaluating the effect of the medium density. Figure 4A,B shows the images before and after lifting the microchip with a PEG-DA concentration of 10%. Figure 4C−F shows the same situation with PEG-DA concentrations of 20 and 30%, respectively. With a higher concentration, the position of PS beads is much different after moving the microchip (Figure 4F) compared with the previous state (Figure 4E). Decreasing the concentration effectively prevented the beads from escaping from the substrate (Figure 4A,B). Therefore, a small concentration of the PEG-DA solution is suggested for bead stabilization.

However, using a concentration that is too low might not be able to cure and hold the hydrogel in shape with insufficient PEG-DA molecules. If the concentration is lower than 10%, then a gel could not be formed. Therefore, the PEG-DA solution was adjusted to 10% and, unless otherwise specified, all following tests were performed using 10% PEG-DA solution.

Effect of the Initial Microchip Position. As discussed, the movement of the microchip would induce flow and destroy the PS bead pattern. Fluid simulations were brought out with the COMSOL Multiphysics (Figure 5A,B). Two-dimensional views were fabricated to show the sectional view. The upper rectangle is filled with air. The lower one, with eight small squares, is filled with water, representing the substrate. A rectangle placed in the middle with an upward transfer shows the microchip. The height of the rectangle is different in these simulations to show the effect of the initial microchip position. Different colors show the strength of the flow velocity.

According to the simulation, flow occurs between the microchip and substrate when the microchip is moved upward. The solution around the microchip would flow into the gap between the microchip and substrate and fill the gap. The initial position of the microchip influences the strength of the flow acting on the beads. In the holes where the PS beads should be patterned, with a lower microchip position (Figure 5A), the flow is much stronger than that with a higher microchip position (Figure 5B).

To experimentally test the effect of the initial microchip position, the microchip was first set at different heights to pattern the beads, and the microchip was lifted out to check the stability of the pattern. From the result shown in Figure 5C, the initial microchip position greatly impacts the stability of the bead pattern: a higher microchip position can guarantee the completeness of the bead pattern. However, the microchip height also decides the DEP force acting on the beads, which should be large enough to drive the beads against the adhesion force from the substrate and drag force from the flow, as shown in eq 4. The previous study[58] shows that, for every 50 μm higher, a 1 V larger voltage input is needed to maintain the strength of the electric field acting on the microparticle. Therefore, with a specific input signal to hold the PS bead pattern, the microchip should be set to a maximum height that can be used to transfer the microbeads.

Effect of the Adhesion. During the manipulation procedure, the DEP force and hydrodynamic force dominate the movement of the beads. However, in the microscale, the adhesion force between microparticles and the force between microparticles and the environment cannot be ignored as it is with the same scale as those macro forces. As reported in the previous study,[56] the morphology and properties of the substrate greatly affect the manipulation of the microparticle through the adhesion force. Therefore, the property of the substrate is changed to test the relationship between the adhesion force and stability of the pattern in this study.

Tween 20 is commonly used for micromanipulation to decrease the adhesion force between microparticles and the environment and as the surfactant to separate the microparticles. In the previous study,[55] Tween 20 was used to weaken the adhesion force between the PS bead and substrate to increase the successful pattern rate. To check the effect caused by the adhesion force, PS beads are suspended in 0,

https://doi.org/10.1021/acsami.4c10675
ACS Appl. Mater. Interfaces 2024, 16, 49973−49984

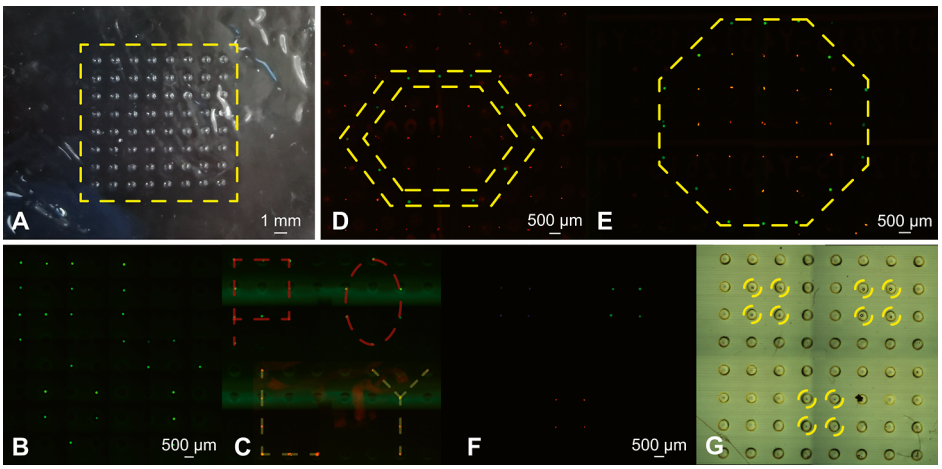

Figure 6. (A) Center part of the cured PEG-DA hydrogel with PS bead patterns. (B) PS bead patterns of a series character of "POLY" with a single type of beads. (C) PS bead patterns of a series character of "POLY" with two types of beads. (D) Hexagon PS bead pattern with two types of beads. (E) Octagon PS bead pattern with two types of beads. (F) PS bead patterns of squares with three types of beads. (G) Microscopic image with transmitted light of the three types of bead patterning.

0.05, and 0.5% Tween 20 solution. According to the result in Figure 5D, the introduction of Tween 20 lowers the attached beads' ratio as the adhesion force is weakened. However, the rate remains even if the concentration increases. This can be explained by that the adhesion force does not lead to the movement of the beads. Therefore, 0.05% Tween 20 is introduced to the solution in this paper to ensure the bead translation when holding the beads with DEP force.

Effect of the Medium Height. The height of the medium is also a factor that might impact the quality of the bead pattern. When the microchip is lifted away from the PEG-DA medium, the medium would also be pulled up, owing to the liquid tension. The existence of liquid tension would lead to the fluctuation of the medium and cause movement of the particles in the medium. To decrease the effect of the liquid tension and stabilize the PS bead pattern, situations with different medium heights were tested in this experiment.

Experiments were conducted to show the difference between the PS bead pattern before and after the microchip is lifted up with the medium height of 1.6 and 2.6 mm, and the result is shown in Figure 5E. It shows that the difference between the medium height clearly influences the stabilization of the PS bead pattern. With a high medium height, the PS bead pattern would barely be destroyed.

Effect of the Particle Size. Figure 5A,B shows the simulation of the procedure for lifting the microchip. The flow happens in the gap between the microchip and the substrate surface. However, for the holes with a 500 μm diameter in the substrate, it would only influence the upper area of the holes, and there is no turbulent flow in the bottom of the holes. For different sizes of the beads, the strength of the flow acting on the beads is also different.

Figure 5F shows the bead attachment rate with different sizes of beads. The pattern for the beads with a 50 μm radius almost retains its shape after removing the microchip. Therefore, to keep the bead pattern, a certain depth of the holes must be maintained for different sizes of beads in the holes.

Verification of the System. The performance of the system is examined experimentally in an adopted environment. Different color PS beads in the 10% PEG-DA and 0.05% Tween-20 solution were used to create single-bead patterns as well as multiple-bead patterns on the substrate and encapsulated by curing the hydrogel solution as shown in Figure 6. As the red beads are smaller than the green beads, the selected concentration would lead to more beads being captured by each electrode, forming a bead cluster for better illustration. Figure 6A shows the curing hydrogel. PS beads are encapsulated in the dotted array circled by the yellow rectangle. Figure 6B shows the formed "POLY" pattern with single green PS beads in an 8 × 8 array. Images were captured and spliced through the Leica microscope. The results with two types of bead patterning are presented in Figure 6C. Images captured through a green filter and a red filter were overlapped and combined. As the red beads are smaller than the green beads, to better show the pattern, for each electrode in the microchip, several red beads were gathered and trapped to form red bead clusters. The bead clusters were then transferred and patterned. To illustrate the ability of the proposed system to pattern different microparticles in a specified form, a hexagonal pattern was fabricated, as shown in Figure 6D. The green beads were patterned to a hexagon, while the red beads were surrounding. An octagon pattern was also formed, as shown in Figure 6E.

An experiment for patterning three different color PS beads with different sizes was conducted, as shown in Figure 6F. For each bead size, a 2 × 2 bead pattern was formed and transferred to the hole grid for trapping. Images captured with different color filters were processed the same as before. The microchip was then lifted and removed for hydrogel curing. Figure 6G was taken through the transmitted light and shows the beads in the holes. Different color beads are highlighted with different color circles.

CONCLUSIONS

This study presents a novel approach to efficiently construct large-scale microparticle patterns and encapsulate them into a hydrogel using a 4-by-4 dot electrode array chip combined with a micromanipulation system. Micro PS beads were selected for patterning on a PMMA substrate featuring an array of holes, controlled via a motorized platform integrated with a microscope. Through the controlled activation of specific electrodes via a relay mechanism, beads were trapped, allowing

https://doi.org/10.1021/acsami.4c10675
ACS Appl. Mater. Interfaces 2024, 16, 49973−49984

the formation of diverse microparticle patterns. These patterns were subsequently transferred to the hole array for stabilization. The pattern was encapsulated into a hydrogel after a large-scale pattern was formed. By employing different colored PS beads, multiple-type bead patterns were achievable. Experimental optimization was conducted to enhance the system efficiency for patterning and stabilizing the formed PS bead patterns before hydrogel curing. The proposed system offers a cost-effective, flexible, and efficient method utilizing nDEP for creating large-scale microparticle patterns encapsulated in a hydrogel. Given the ubiquitous applicability of DEP in manipulating microparticles, the results suggest the potential applicability of the nDEP patterning technique in diverse bioparticle postprocess analytics.

AUTHOR INFORMATION

Corresponding Author

Henry Kar Hang Chu − *Department of Mechanical Engineering, The Hong Kong Polytechnic University, Hong Kong SAR 999077, China*; Email: henry.chu@polyu.edu.hk

Authors

Kaicheng Huang − *Department of Materials Science and Engineering, Southern University of Science and Technology, Shenzhen, Guangdong 518055, China; Shenzhen Key Laboratory of Nanoimprint Technology, Southern University of Science and Technology, Shenzhen, Guangdong 518055, China; Department of Mechanical Engineering, The Hong Kong Polytechnic University, Hong Kong SAR 999077, China*; orcid.org/0000-0003-0446-9722

Jiewen Lai − *Department of Mechanical Engineering, The Hong Kong Polytechnic University, Hong Kong SAR 999077, China; Electronic Engineering Department, The Chinese University of Hong Kong, Hong Kong SAR 999077, China*

Hongliang Ren − *Electronic Engineering Department, The Chinese University of Hong Kong, Hong Kong SAR 999077, China*

Chunhui Wu − *Department of Materials Science and Engineering, Southern University of Science and Technology, Shenzhen, Guangdong 518055, China; Shenzhen Key Laboratory of Nanoimprint Technology, Southern University of Science and Technology, Shenzhen, Guangdong 518055, China*

Xing Cheng − *Department of Materials Science and Engineering, Southern University of Science and Technology, Shenzhen, Guangdong 518055, China; Shenzhen Key Laboratory of Nanoimprint Technology, Southern University of Science and Technology, Shenzhen, Guangdong 518055, China*

Complete contact information is available at: https://pubs.acs.org/10.1021/acsami.4c10675

Notes

The authors declare no competing financial interest.

ACKNOWLEDGMENTS

The work was financially supported in part by the Research Grant Council of the Hong Kong Special Administrative Region (grant no. 25204016), Guangdong-Hong Kong-Macau Joint Laboratory on Micro−Nano Manufacturing Technology (grant no. 2021LSYS004), National Natural Science Foundation of China (grant no. 62403231), and National Natural Science Foundation of China (grant no. 31927802).

REFERENCES

(1) Deng, K.; Du, P.; Liu, K.; Tao, X.; Harati, J.; Jhang, J.-W.; Kim, J.; Wang, P.-Y. Programming colloidal self-assembled patterns (cSAPs) into thermo-responsible hybrid surfaces for controlling human stem cells and macrophages. *ACS Appl. Mater. Interfaces* **2021**, *13*, 18563−18580.

(2) Hanke, C.; Dittrich, P. S.; Reyes, D. R. Dielectrophoretic cell capture on polyester membranes. *ACS Appl. Mater. Interfaces* **2012**, *4*, 1878−1882.

(3) Naoumi, N.; Michaelidou, K.; Papadakis, G.; Simaiaki, A. E.; Fernández, R.; Calero, M.; Arnau, A.; Tsortos, A.; Agelaki, S.; Gizeli, E. Acoustic array biochip combined with allele-specific PCR for multiple cancer mutation analysis in tissue and liquid biopsy. *ACS Sens.* **2022**, *7*, 495−503.

(4) Li, S.; Coffinier, Y.; Lagadec, C.; Cleri, F.; Nishiguchi, K.; Fujiwara, A.; Kim, S. H.; Clément, N. Single-cell electrochemical aptasensor array. *ACS Sens.* **2023**, *8*, 2921−2926.

(5) Liu, C.; Qie, Y.; Zhao, L.; Li, M.; Guo, L.-H. A high-throughput platform for the rapid quantification of phosphorylated histone H2AX in cell lysates based on microplate electrochemiluminescence immunosensor array. *ACS Sens.* **2021**, *6*, 3724−3732.

(6) Zhu, K.; Wang, Z.; Zong, S.; Liu, Y.; Yang, K.; Li, N.; Wang, Z.; Li, L.; Tang, H.; Cui, Y. Hydrophobic plasmonic nanoacorn array for a label-free and uniform SERS-based biomolecular assay. *ACS Appl. Mater. Interfaces* **2020**, *12*, 29917−29927.

(7) Weng, Z.; You, Z.; Li, H.; Wu, G.; Song, Y.; Sun, H.; Fradlin, A.; Neal-Harris, C.; Lin, M.; Gao, X.; et al. CRISPR-Cas12a Biosensor Array for Ultrasensitive Detection of Unamplified DNA with Single-Nucleotide Polymorphic Discrimination. *ACS Sens.* **2023**, *8*, 1489−1499.

(8) Mitchell, L.; Shen, C.; Timmins, H. C.; Park, S. B.; New, E. J. A versatile fluorescent sensor array for platinum anticancer drug detection in biological fluids. *ACS Sens.* **2021**, *6*, 1261−1269.

(9) Elkeles, T.; Park, S.; Werner, J. G.; Weitz, D. A.; Yossifon, G. Dielectrophoretic characterization of dynamic microcapsules and their magnetophoretic manipulation. *ACS Appl. Mater. Interfaces* **2022**, *14*, 15765−15773.

(10) Peng, W.; Datta, P.; Ayan, B.; Ozbolat, V.; Sosnoski, D.; Ozbolat, I. T. 3D bioprinting for drug discovery and development in pharmaceutics. *Acta Biomater.* **2017**, *57*, 26−46.

(11) Pethig, R. Review Article—Dielectrophoresis: Status of the theory, technology, and applications. *Biomicrofluidics* **2010**, *4*, 022811.

(12) Ramón-Azcón, J.; Yasukawa, T.; Lee, H. J.; Matsue, T.; Sánchez-Baeza, F.; Marco, M.-P.; Mizutani, F. Competitive multi-immunosensing of pesticides based on the particle manipulation with negative dielectrophoresis. *Biosens. Bioelectron.* **2010**, *25*, 1928−1933.

(13) Yamamoto, M.; Yasukawa, T.; Suzuki, M.; Kosuge, S.; Shiku, H.; Matsue, T.; Mizutani, F. Patterning with particles using three-dimensional interdigitated array electrodes with negative dielectrophoresis and its application to simple immunosensing. *Electrochim. Acta* **2012**, *82*, 35−42.

(14) Lee, H. J.; Yasukawa, T.; Shiku, H.; Matsue, T. Rapid and separation-free sandwich immunosensing based on accumulation of microbeads by negative-dielectrophoresis. *Biosens. Bioelectron.* **2008**, *24*, 1000−1005.

(15) Lee, H. J.; Lee, S. H.; Yasukawa, T.; Ramón-Azcón, J.; Mizutani, F.; Ino, K.; Shiku, H.; Matsue, T. Rapid and simple immunosensing system for simultaneous detection of tumor markers based on negative-dielectrophoretic manipulation of microparticles. *Talanta* **2010**, *81*, 657−663.

(16) Ramón-Azcón, J.; Yasukawa, T.; Mizutani, F. Sensitive and spatially multiplexed detection system based on dielectrophoretic manipulation of DNA-encoded particles used as immunoreactions platform. *Anal. Chem.* **2011**, *83*, 1053−1060.

(17) Honegger, T.; Peyrade, D. Dielectrophoretic properties of engineered protein patterned colloidal particles. *Biomicrofluidics* **2012**, *6*, 44115.
(18) Sund, J.; Alenius, H.; Vippola, M.; Savolainen, K.; Puustinen, A. Proteomic characterization of engineered nanomaterial−protein interactions in relation to surface reactivity. *ACS Nano* **2011**, *5*, 4300−4309.
(19) Mansuy-Schlick, V.; Delage-Mourroux, R.; Jouvenot, M.; Boireau, W. Strategy of macromolecular grafting onto a gold substrate dedicated to protein−protein interaction measurements. *Biosens. Bioelectron.* **2006**, *21*, 1830−1837.
(20) Wu, L. Y.; Ross, B. M.; Hong, S.; Lee, L. P. Bioinspired nanocorals with decoupled cellular targeting and sensing functionality. *Small* **2010**, *6*, 503−507.
(21) Wu, C.; Chen, R.; Liu, Y.; Yu, Z.; Jiang, Y.; Cheng, X. A planar dielectrophoresis-based chip for high-throughput cell pairing. *Lab Chip* **2017**, *17*, 4008−4014.
(22) Haeberle, S.; Zengerle, R. Microfluidic platforms for lab-on-a-chip applications. *Lab Chip* **2007**, *7*, 1094−1110.
(23) Lim, Y.; Kouzani, A.; Duan, W. Lab-on-a-chip: a component view. *Microsyst. Technol.* **2010**, *16*, 1995−2015.
(24) Okochi, M.; Takano, S.; Isaji, Y.; Senga, T.; Hamaguchi, M.; Honda, H. Three-dimensional cell culture array using magnetic force-based cell patterning for analysis of invasive capacity of BALB/3T3/v-src. *Lab Chip* **2009**, *9*, 3378−3384.
(25) Albrecht, D. R.; Sah, R. L.; Bhatia, S. N. Geometric and material determinants of patterning efficiency by dielectrophoresis. *Biophys. J.* **2004**, *87*, 2131−2147.
(26) Albrecht, D.; Tsang, V.; Sah, R.; Bhatia, S. Photo- and electropatterning of hydrogel-encapsulated living cell arrays. *Lab Chip* **2005**, *5*, 111.
(27) Gagnon, Z.; Mazur, J.; Chang, H. C. Integrated AC electrokinetic cell separation in a closed-loop device. *Lab Chip* **2010**, *10*, 718.
(28) Jeon, H.; Lee, D.-H.; Jundi, B.; Pinilla-Vera, M.; Baron, R. M.; Levy, B. D.; Voldman, J.; Han, J. Fully automated, sample-to-answer leukocyte functional assessment platform for continuous sepsis monitoring via microliters of blood. *ACS Sens.* **2021**, *6*, 2747−2756.
(29) El-Ali, J.; Sorger, P. K.; Jensen, K. F. Cells on chips. *Nature* **2006**, *442*, 403−411.
(30) Tian, Z.; Wang, Z.; Zhang, P.; Naquin, T. D.; Mai, J.; Wu, Y.; Yang, S.; Gu, Y.; Bachman, H.; Liang, Y.; et al. Generating multifunctional acoustic tweezers in Petri dishes for contactless, precise manipulation of bioparticles. *Sci. Adv.* **2020**, *6*, No. eabb0494.
(31) Zhang, S.; Zhai, Y.; Peng, R.; Shayegannia, M.; Flood, A. G.; Qu, J.; Liu, X.; Kherani, N. P.; Wheeler, A. R. Assembly of topographical micropatterns with optoelectronic tweezers. *Adv. Opt. Mater.* **2019**, *7*, 1900669.
(32) Chen, X.; Chen, X.; Elsayed, M.; Edwards, H.; Liu, J.; Peng, Y.; Zhang, H.; Zhang, S.; Wang, W.; Wheeler, A. R. Steering micromotors via reprogrammable optoelectronic paths. *ACS Nano* **2023**, *17*, 5894−5904.
(33) Sims, C. E.; Allbritton, N. L. Analysis of single mammalian cells on-chip. *Lab Chip* **2007**, *7*, 423−440.
(34) Zhou, J.; Wu, Y.; Lee, S.-K.; Fan, R. High-content single-cell analysis on-chip using a laser microarray scanner. *Lab Chip* **2012**, *12*, 5025−5033.
(35) Ino, K.; Shiku, H.; Ozawa, F.; Yasukawa, T.; Matsue, T. Manipulation of microparticles for construction of array patterns by negative dielectrophoresis using multilayered array and grid electrodes. *Biotechnol. Bioeng.* **2009**, *104*, 709−718.
(36) Dutta, S.; Singh, A. K.; Pattader, P. S. G.; Bandyopadhyay, D. Genesis of electric field assisted microparticle assemblage in a dielectric fluid. *J. Fluid Mech.* **2021**, *915*, A6.
(37) Chu, H.; Huan, Z.; Mills, J.; Yang, J.; Sun, D. Three-dimensional cell manipulation and patterning using dielectrophoresis via a multi-layer scaffold structure. *Lab Chip* **2015**, *15*, 920−930.
(38) Kim, D.; Sonker, M.; Ros, A. Dielectrophoresis: From molecular to micrometer-scale analytes. *Anal. Chem.* **2019**, *91*, 277−295.
(39) Sun, M.; Durkin, P.; Li, J.; Toth, T. L.; He, X. Label-free on-chip selective extraction of cell-aggregate-laden microcapsules from oil into aqueous solution with optical sensor and dielectrophoresis. *ACS Sens.* **2018**, *3*, 410−417.
(40) Yasukawa, T.; Shiku, H.; Matsue, T.; Mizutani, F. Rapid and simple immunoassay based on negative dielectrophoresis with three-dimensional interdigitated array electrodes. *ECS Trans.* **2013**, *50*, 139−146.
(41) Menad, S.; Franqueville, L.; Haddour, N.; Buret, F.; Frenea-Robin, M. nDEP-driven cell patterning and bottom-up construction of cell aggregates using a new bioelectronic chip. *Acta Biomater.* **2015**, *17*, 107−114.
(42) Yafouz, B.; Kadri, N. A.; Ibrahim, F. The design and simulation of a planar microarray dot electrode for a dielectrophoretic lab-on-chip device. *Int. J. Electrochem. Sci.* **2012**, *7*, 12054−12063.
(43) Abdallat, R. G.; Tajuddin, A. S. A.; Gould, D. H.; Hughes, M. P.; Fatoyinbo, H. O.; Labeed, F. H. Process development for cell aggregate arrays encapsulated in a synthetic hydrogel using negative dielectrophoresis. *Electrophoresis* **2013**, *34*, 1059−1067.
(44) Bajaj, P.; Marchwiany, D.; Duarte, C.; Bashir, R. Patterned three-dimensional encapsulation of embryonic stem cells using dielectrophoresis and stereolithography. *Adv. Healthcare Mater.* **2013**, *2*, 450−458.
(45) Chiang, M.-Y.; Hsu, Y.-W.; Hsieh, H.-Y.; Chen, S.-Y.; Fan, S.-K. Constructing 3D heterogeneous hydrogels from electrically manipulated prepolymer droplets and crosslinked microgels. *Sci. Adv.* **2016**, *2*, No. e1600964.
(46) Li, Y.; Lai, S. H.; Liu, N.; Zhang, G.; Liu, L.; Lee, G.-B.; Li, W. J. Fabrication of high-aspect-ratio 3D Hydrogel microstructures using optically induced electrokinetics. *Micromachines* **2016**, *7*, 65.
(47) Nestor, B.; Samiei, E.; Samanipour, R.; Gupta, A.; Van den Berg, A.; de Leon Derby, M. D.; Wang, Z.; Nejad, H. R.; Kim, K.; Hoorfar, M. Digital microfluidic platform for dielectrophoretic patterning of cells encapsulated in hydrogel droplets. *RSC Adv.* **2016**, *6*, 57409−57416.
(48) Ramón-Azcón, J.; Ahadian, S.; Obregón, R.; Camci-Unal, G.; Ostrovidov, S.; Hosseini, V.; Kaji, H.; Ino, K.; Shiku, H.; Khademhosseini, A.; et al. Gelatin methacrylate as a promising hydrogel for 3D microscale organization and proliferation of dielectrophoretically patterned cells. *Lab Chip* **2012**, *12*, 2959−2969.
(49) Suzuki, M.; Yasukawa, T.; Shiku, H.; Matsue, T. Negative dielectrophoretic patterning with colloidal particles and encapsulation into a hydrogel. *Langmuir* **2007**, *23*, 4088−4094.
(50) Yue, T.; Nakajima, M.; Tajima, H.; Kojima, M.; Fukuda, T. High speed cell manipulation by dielectrophoresis and movable microstructure embedding cells fabricated inside microfluidic chips; IEEE, 2012, pp 938−943.*2012 IEEE/RSJ International Conference on Intelligent Robots and Systems*
(51) Zhang, Y.; Jiang, W.; Gu, T.; Han, J.; Lei, B.; Wang, L.; Liu, H.; Yin, L.; Chen, B.; Shi, Y. Multidomain Oriented Particle Chains Based on Spatial Electric Field and Their Optical Application. *Langmuir* **2020**, *36*, 11546−11555.
(52) Zhang, S.; Li, W.; Elsayed, M.; Peng, J.; Chen, Y.; Zhang, Y.; Zhang, Y.; Shayegannia, M.; Dou, W.; Wang, T.; et al. Integrated Assembly and Photopreservation of Topographical Micropatterns. *Small* **2021**, *17*, 2103702.
(53) Zhang, Y.; Zheng, X.; Jiang, W.; Han, J.; Pu, J.; Wang, L.; Lei, B.; Chen, B.; Shi, Y.; Yin, L.; et al. Formation of highly ordered micro fillers in polymeric matrix by electro-field-assisted aligning. *RSC Adv.* **2019**, *9*, 15238−15245.
(54) Huang, K.; Cui, Z.; Ajamieh, I. A.; Lai, J.; Mills, J. K.; Chu, H. K. Automated Single-microparticle Patterning System for Micro-analytics; IEEE, 2020, pp 390−396.*2020 IEEE 16th International Conference on Automation Science and Engineering (CASE)*
(55) Huang, K.; Cui, Z.; Lai, J.; Lu, B.; Chu, H. K. Optimization of a single-particle micropatterning system with robotic nDEP-tweezers.

IEEE Transactions on Automation Science and Engineering **2022**, *19*, 818−832.
(56) Huang, K.; Lu, B.; Lai, J.; Chu, H. K. H. Microchip System for Patterning Cells on Different Substrates via Negative Dielectrophoresis. *IEEE Trans. Biomed. Circ. Syst.* **2019**, *13*, 1063−1074.
(57) Pohl, H. A. *Dielectrophoresis: The Behavior of Neutral Matter in Nonuniform Electric Fields (Cambridge Monographs on Physics)*; Cambridge University Press: Cambridge/New York, 1978.
(58) Huang, K.; Ajamieh, I. A.; Cui, Z.; Lai, J.; Mills, J. K.; Chu, H. K. Automated embryo manipulation and rotation via robotic nDEP-tweezers. *IEEE Trans. Biomed. Eng.* **2021**, *68*, 2152−2163.

https://doi.org/10.1021/acsami.4c10675
ACS Appl. Mater. Interfaces 2024, 16, 49973−49984